

## Conclusions

In this study we demonstrate the utility of VCD as a new biophysical technique for studying ligand binding in metallo-enzymes. Because of the sensitivity of VCD to energetically small interactions between the azide ligand and the E7 and E11 distal residues, which provide a chiral environment for the prochiral azide ligand, VCD studies have the potential to provide a new view of the subtle molecular interactions that influence ligand binding. Although other possibilities cannot be ruled out, our analysis strongly suggests that the source of the enhanced magnetic dipole strength is vibrationally induced current in the delocalized electrons of the heme plane. In the context of this interpretation, the results

of these experiments reveal the presence of a long-range electronic communication between the heme, its ligands, and the distal protein residues to which VCD is sensitive.

**Acknowledgment.** We thank Dr. Curt Marcott for help in the early stages of this work. We gratefully acknowledge support for this work from NIH Grants IR01GM30741-09 (to S.A.A.), GM23567 (to L.A.N. and T.B.F.), 5P01-HL40453 (to R.W.N.), GM33775 and GM31756 (to S.G.S.), GM18894 (to N.-T.Y.), and GM27738 (to S.G.B.). We also acknowledge support for this work by the Fond der Chemischen Industrie and the Medizinische Biophysik e.V. (to K.G.).

## Solid-State NMR Studies of the Molecular Motion in the Kaolinite:DMSO Intercalate

Melinda J. Duer,\* João Rocha, and Jacek Klinowski

Contribution from the Department of Chemistry, University of Cambridge, Lensfield Road, Cambridge CB2 1EW, U.K. Received July 15, 1991

**Abstract:** The structure and motion of the guest molecule in the interlayer space of the kaolinite:DMSO intercalation compound have been studied by  $^2\text{H}$  NMR spectroscopy of static samples,  $^{13}\text{C}$ ,  $^{27}\text{Al}$ , and  $^{29}\text{Si}$  high-resolution solid-state NMR spectroscopies, variable-temperature powder X-ray diffraction, and Fourier transform infrared spectroscopy. The guest DMSO molecules are hydrogen-bonded via the oxygen atom to the kaolinite hydroxyls which face the interlayer space, and there is a degree of interaction between the sulfur atom of the DMSO molecule and the siliceous matrix of kaolinite. There are two independent sites for the DMSO methyl groups with effective  $^2\text{H}$  quadrupole coupling constants of 59 and 67 kHz, and the population of at least one site is in motion. The difference in these couplings probably reflects different geometries of the methyl groups in the two sites, caused by their partial "keying" into the siliceous matrix. Three motional models produce simulations which are in acceptable agreement with the experimental spectra. One fit is consistent with the keying of one methyl group of a DMSO molecule into the kaolinite layer and raises an interesting point concerning the packing of the DMSO molecules in the interlayer spacing. Above ca. 339 K further exchange processes must be taken into account in  $^2\text{H}$  NMR line shape simulations and may trigger structural transformations of the intercalate.

## Introduction

Intercalation of clays such as kaolinite has led to the development of materials with novel rheological, surface, and structural properties which have found applications in the paper industry, in polymer composites, as matrices for slow release of trapped molecules, and as soil conditioners.<sup>1-3</sup> Kaolinite is a dioctahedral (1:1) layered aluminosilicate with the chemical formula  $\text{Si}_2\text{O}_5(\text{OH})_4\text{Al}_2$ . The kaolinite layer can be regarded as the result of a fusion of the  $(\text{Si}_2\text{O}_5)_n^{2-}$  layer and the  $\text{Al}(\text{OH})_3$  (gibbsite) layer (Figure 1). Wada<sup>4</sup> has found that inorganic salts such as potassium acetate penetrate the interlayer space of kaolinite. Small and highly polar molecules such as dimethyl sulfoxide (DMSO) can also be directly intercalated into kaolinite. These results have triggered a considerable amount of research into the formation and structure of the interlayer complexes of kaolinite.

Some attention has been given to the structure of the kaolinite:DMSO intercalate,<sup>5-14</sup> and several solid-state NMR studies

have appeared.<sup>10-14</sup> However, there has been no study of the molecular motion of DMSO in the interlayer space, which may be an important factor in determining the structure and properties of the intercalation compound. Upon intercalation, the (001) kaolinite lattice spacing increases from 7.17 to 11.26 Å, and this increase in spacing has been used to differentiate between kaolinite and serpentinite group minerals. Unfortunately, suitable single crystals of kaolinite are not available. Further, because of peak overlap the Rietveld method<sup>15</sup> is of limited value for structures with large, low-symmetry unit cells. However, infrared (IR) and NMR studies can supplement the structural information available from X-ray diffraction (XRD).<sup>12</sup> The two published attempts to solve the kaolinite:DMSO intercalate structure used quasi-single-crystal methods in tandem with IR and solid-state NMR

(1) Theng, B. K. G. In *The Chemistry of Clay-Organic Reactions*; Adam-Hilger: London, 1974.

(2) Theng, B. K. G. *Clays Clay Miner.* **1982**, *30*, 1.

(3) Lagaly, G. *Philos. Trans. R. Soc. London* **1984**, *A311*, 315.

(4) Wada, K. *Am. Mineral.* **1961**, *46*, 78.

(5) Weiss, A.; Thielepape, W.; Orth, H. In *Proceedings of the International Clay Conference*, Jerusalem; Heller, L., Weiss, A., Eds.; Israel Program for Scientific Translations: Jerusalem, 1966; Vol. 1, p 277.

(6) Olejnik, S.; Aylmore, L. A. G.; Postner, A. M.; Quirk, J. P. *J. Phys. Chem.* **1968**, *72*, 241.

(7) Sanchez Camazano, M.; Gonzalez Garcia, G. *An. Edafol. Agrobiol.* **1970**, *29*, 651.

(8) Jacobs, H.; Sterckx, M. In *Proceedings of the Reunion Hispano-Belge Miner. Arg.*, Madrid; Serratos, J. M., Ed.; CSIC: Madrid, 1970; p 154.

(9) Adams, J. M.; Walt, G. *Clays Clay Miner.* **1980**, *28*, 173.

(10) Thompson, J. G. *Clays Clay Miner.* **1985**, *33*, 173.

(11) Thompson, J. G.; Cuff, C. *Clays Clay Miner.* **1985**, *33*, 490.

(12) Raupach, M.; Barron, P. F.; Thompson, J. G. *Clays Clay Miner.* **1987**, *35*, 208.

(13) Duer, M. J.; Klinowski, J.; Rocha, J. The Study of Intercalated Molecules Using One- and Two-Dimensional Solid-State NMR. Ampère Conference, Stuttgart, September 1990.

(14) Rocha, J.; Kolodziejewski, W.; Klinowski, J. *Chem. Phys. Lett.* **1991**, *176*, 395.

(15) Rietveld, H. M. *J. Appl. Crystallogr.* **1969**, *30*, 65.

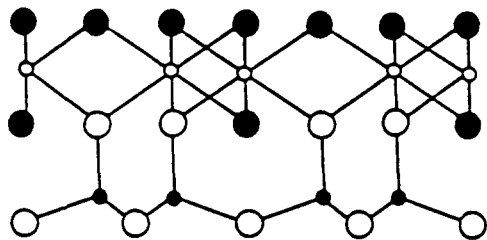


Figure 1. The structure of one kaolinite layer. Small and large open circles denote Al and O atoms, respectively; small and large solid circles denote Si atoms and hydroxyl groups, respectively.

spectroscopies.<sup>11,12</sup> By analogy with the kaolinite:DMSO intercalation compound, the structure was found to be C-face centered P1. Each DMSO molecule is triply hydrogen-bonded above the octahedral vacancy in the gibbsite sheet of the kaolinite layer. One methyl group is keyed into the ditrigonal hole in the tetrahedral sheet with the other S-C bond parallel to the sheet.

We have studied the intercalate using <sup>2</sup>H NMR spectroscopy of static samples, high-resolution <sup>13</sup>C, <sup>27</sup>Al, and <sup>29</sup>Si magic-angle-spinning (MAS) NMR spectroscopies, and variable-temperature XRD and FTIR spectroscopy. Analysis of the <sup>2</sup>H line shapes yields much information about the motional modes of the DMSO molecule, from which details of molecular orientation within the kaolinite layers can be obtained.

### Experimental Section

**Sample Preparation.** We have used highly crystalline (Hinckley index<sup>16</sup> 1.24) and pure (<3 wt % mica, <0.40 wt % Fe<sub>2</sub>O<sub>3</sub>) Cornish kaolinite with a specific surface area (BET, N<sub>2</sub>) of 9.8 m<sup>2</sup> g<sup>-1</sup> and a cation-exchange capacity (determined by saturation with ammonium acetate) of 4.0 mequiv/100 g. Approximately 80% of the particles were smaller than 2 μm. DMSO and DMSO-*d*<sub>6</sub> were intercalated as follows. The organic (30 cm<sup>3</sup>) was added to 300 mg of kaolinite. The suspension was placed in an ultrasonic bath for 15 min and then allowed to react without stirring at room temperature for 56 days. In some experiments the reaction was carried out at 50 °C for 10 days with stirring. Deuteration of kaolinite:DMSO (*d*-kaolinite:DMSO) was carried out by mixing 30 cm<sup>3</sup> of DMSO with 300 mg of kaolinite and 3 cm<sup>3</sup> of <sup>2</sup>H<sub>2</sub>O. The suspension was placed in an ultrasonic bath for 15 min, after which it was allowed to react without stirring at room temperature for 56 days. The samples were finally dried at 50 °C for 7 days.

**Techniques.** XRD patterns were recorded on a Philips PW1710 automated powder diffractometer equipped with a graphite monochromator and a vertical goniometer using Cu Kα radiation (λ = 1.5418 Å). Variable-temperature studies were carried out using an Anton-Parr high-temperature attachment in a N<sub>2</sub> atmosphere, with a heating rate of 2 deg min<sup>-1</sup> and an equilibration time of 10 min at each temperature; the rate of quenching from 553 to 293 K was 10 deg min<sup>-1</sup>.

FTIR spectra in the region 4000–400 cm<sup>-1</sup> were measured on a Nicolet MX-1 spectrometer using the conventional KBr technique. The spectra were typically an average of 128 scans with 1-cm<sup>-1</sup> resolution.

Solid-state NMR spectra were recorded on a Bruker MSL-400 multinuclear spectrometer. <sup>27</sup>Al spectra were recorded with <sup>1</sup>H high-power decoupling (HPDC) at 104.26 MHz using very short, 0.6-μs (equivalent to π/20) radio frequency (rf) pulses, 0.5-s recycle delays, and spinning rates of 10–13 kHz. Chemical shifts are quoted in ppm from external Al(H<sub>2</sub>O)<sub>6</sub><sup>3+</sup>. <sup>1</sup>H-<sup>29</sup>Si CP/MAS spectra were measured at 79.50 MHz using a <sup>1</sup>H π/2 pulse of 6.0 μs, single contacts, an (optimized) contact time of 6 ms, recycle delays of 2 s and spinning rates of 3.5–4.0 kHz. The Hartmann-Hahn condition was established using kaolinite.<sup>17</sup> High-power-decoupled <sup>29</sup>Si spectra were recorded using π/4 rf pulses and 30-s recycle delays. Chemical shifts are quoted in ppm from external TMS. <sup>1</sup>H-<sup>13</sup>C CP/MAS spectra were measured at 100.61 MHz using a <sup>1</sup>H π/2 pulse of 5.0 μs, single contacts, an (optimized) contact time of 5 ms, recycle delays of 2 s, and spinning rates usually of 3.5–4.0 kHz. <sup>13</sup>C HPDC spectra were acquired using π/4 rf pulses and 20-s recycle delays. Chemical shifts are quoted in ppm from external TMS. Static <sup>2</sup>H spectra were recorded at 61.42 MHz, using π/2 pulses of 4.0–5.0 μs and a recycle delay of 1 s, in the temperature range 160–415 K, using the quadrupole echo pulse sequence, (π/2)<sub>x</sub>-τ<sub>1</sub>-(π/2)<sub>y</sub>-τ<sub>2</sub>-acquisition. Spectra for sev-

eral values of τ<sub>1</sub> were acquired at each temperature, with τ<sub>2</sub> generally 4 μs longer than τ<sub>1</sub>, to take into account finite pulse widths.

### Simulation of the Static <sup>2</sup>H Spectra<sup>18–20</sup>

**Theory.** In a system where exchange is possible between *N* equivalent sites, the time evolution of the (complex) transverse components of magnetization {M<sup>+</sup>(*t*)<sub>*j*</sub>} of each of the *j* sites may be expressed in matrix form:

$$\frac{d\mathbf{M}^+(t)}{dt} = [i\mathbf{\Omega} + \mathbf{K}]\mathbf{M}^+(t) \\ = \mathbf{A}\mathbf{M}^+(t) \quad (1)$$

where M<sup>+</sup>(*t*) is an *N*-dimensional vector whose components are the transverse magnetizations associated with each of the *N* sites at a time *t*. Conventionally, the real parts of the complex elements of M<sup>+</sup>(*t*) correspond to the *x*-components of magnetization, and the imaginary parts to the *y*-components. Ω is a diagonal *N* × *N* matrix whose elements are the resonance frequencies of each of the *N* sites, and K is a kinetic matrix which describes the motion of magnetization between the *N* sites. The general solution of eq 1 is

$$\mathbf{M}^+(t) = \mathbf{M}^+(t'=0) \exp(\mathbf{A}t) \quad (2)$$

The conclusion is that the time evolution of the transverse magnetizations depends on the initial components at *t* = 0, M<sup>+</sup>(*t*=0), which in turn depend on the pulse sequence that produced the transverse magnetization. The echo pulse sequence (π/2)<sub>x</sub>-τ<sub>1</sub>-(π/2)<sub>y</sub>-τ<sub>2</sub>-acquisition (*t*) yields initial transverse magnetization which depends on the delays τ<sub>1</sub> and τ<sub>2</sub>. The magnetization is

$$\mathbf{M}^+(\tau_1, \tau_2; t'=0) = \exp(\mathbf{A}\tau_2) \exp(\mathbf{A}^*\tau_1) \mathbf{M}^+(0) \quad (3)$$

from solution of eq 1, assuming that the first (π/2)<sub>x</sub> pulse converts all of the original *z*-magnetization to *x*-magnetization, and that the second refocusing pulse changes the sign of the coherences. The elements of M<sup>+</sup>(0) are the initial transverse magnetizations after the first π/2 pulse associated with each of the *N* sites. They are, therefore, simply 1/*N*, if there is equal probability of occupation of each of the sites. The FID resulting after the echo pulse sequence is obtained by summing the transverse magnetization from each of the *N* sites, which in turn are obtained from eqs 2 and 3:

$$\mathbf{F}(\tau_1, \tau_2; t') = \mathbf{1} \cdot \mathbf{M}^+(\tau_1, \tau_2; t') \\ = \mathbf{1} \cdot \exp(\mathbf{A}t') \exp(\mathbf{A}\tau_2) \exp(\mathbf{A}^*\tau_1) \mathbf{M}^+(0) \quad (4)$$

This is easily evaluated once Ω and K are known. K is determined only by the form and speed of the motion.<sup>18,20</sup> The diagonal elements of Ω are simply the resonance frequencies of the *N* sites involved in the motion. They are easily calculated from an input quadrupole tensor referred to a molecular axis frame using standard second-rank tensor transformation techniques. The complete calculation of a powder spectrum involves summing FIDs from all molecular orientations, line broadening, and subsequent Fourier transformation. Finally the spectra for the two possible transitions for spin *I* = 1 must be summed to produce a simulated powder spectrum. The calculation also takes into account the effects of finite 90° pulse widths on the spectrum. All the calculations were carried out with our own computer program.<sup>21</sup>

Summation over molecular orientations in the time domain, rather than the frequency domain, is preferable, because calculations in the frequency domain give rise to singularities and

(18) Abragam, A. *Principles of Nuclear Magnetism*; Oxford Univ Press: Oxford, 1961.

(19) Spiess, H. W. *Chem. Phys.* **1974**, *6*, 217.

(20) Greenfield, M. S.; Ronemus, A. D.; Vold, R. L.; Vold, R. R.; Ellis, P. D.; Raidy, T. E. *J. Magn. Reson.* **1987**, *72*, 89.

(21) CARLA (Computer Aided Resonance Lineshape Analysis), a FORTRAN program by Duer, M. J.

(16) Hinckley, D. N. In *Clays and Clay Minerals*, Proceedings of the 11th national Conference, Ottawa, Ontario; Swineford, A., Ed.; Pergamon Press: New York, 1963; p 299.

(17) Rocha, J.; Klinowski, J. *J. Magn. Reson.* **1990**, *90*, 567.

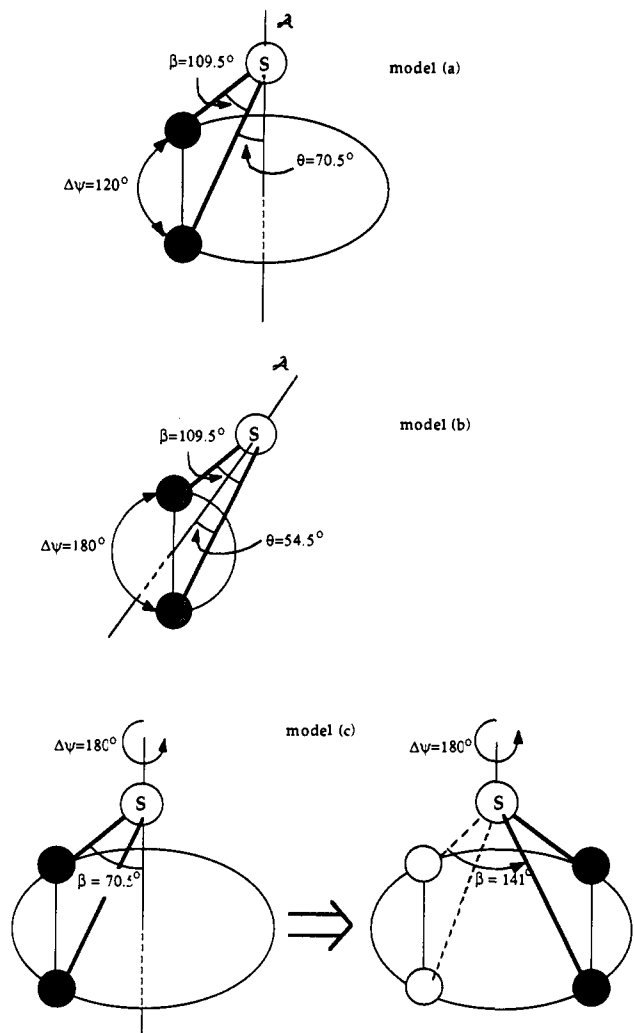


Figure 2. The models of molecular motion used for simulating  $^2\text{H}$  NMR line shapes (see text). "A" is the hop axis for the particular motion. Solid circles denote methyl groups.

spurious features which are not readily identifiable, but which can dominate the spectrum.<sup>22</sup> Of course, the problem in the time domain is that some components continue to oscillate at  $t \rightarrow \infty$ . Therefore, the truncation of the time domain leads to characteristic distortions of the spectra upon Fourier transformation. This problem is easily overcome by multiplying the calculated FID by a decaying function prior to Fourier transformation.

The dependence of the spectrum on the echo delay time  $\tau$  in eq 4 is very useful when fitting calculated spectra to experimental spectra. In the region of  $\tau \sim \tau_c$ , where  $\tau_c$  is the correlation time for the molecular motion in the experimental sample, the line shapes obtained vary with  $\tau$  in a manner determined by the form of the motion. This factor has removed much of the ambiguity associated with the fitting process.

**Molecular Motion Models.** Theoretical line shapes were calculated for five different models of molecular motion (see Figure 2): (a) The two methyl groups hopping about an axis inclined at  $\theta = 70.5^\circ$  to the S-C bonds in jumps  $\Delta\psi = 120^\circ$ , such that the methyl groups jump through an angle  $\beta = 109.5^\circ$ . (b) The two methyl groups hopping about an axis inclined at  $\theta = 54.5^\circ$  to the S-C bonds in jumps  $\Delta\psi = 180^\circ$ , such that the methyl groups again jump through an angle of  $\beta = 109.5^\circ$ . (c) The two methyl groups hopping about an axis inclined at  $\theta = 70.5^\circ$  to the S-C bonds in jumps  $\Delta\psi = 180^\circ$ , such that the methyl groups jump through an angle of  $\beta = 141^\circ$ . (d) As in model b, but with simultaneous wobbling of the flip axis, which is assumed to be

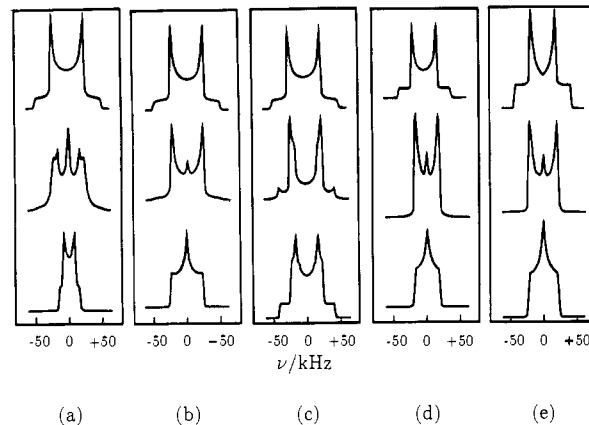


Figure 3. Simulated  $^2\text{H}$  line shapes for each of the five motional models (see text). The hopping frequencies used in the simulations are as follows: top,  $10^3$  Hz; middle,  $10^5$  Hz; and bottom,  $10^7$  Hz. In models d and e the wobbling motion of the flip/bond axis is  $10^7$  Hz. The echo delay  $\tau$  is 25  $\mu\text{s}$ .

confined to a cone of half-angle  $25^\circ$ . The cone is defined by seven sites, six of which define a hexagon around the perimeter of the cone, and one is at the center of the cone. Random hops are assumed to occur between nearest neighbor sites within the cone, with a correlation time  $\tau_c^D$ , which is different from the correlation time for hops about the flip axis,  $\tau_c^J$ . (e) As in model b, but with simultaneous wobbling of the S-C bonds. Once again, the wobbling of this axis was assumed to be confined to a cone, as in model d.

All models assume very rapid rotation of the methyl groups about the S-C axis. In cases where the quadrupole interaction tensor is axial, such motion partially averages the effective quadrupole coupling constant by the factor

$$\frac{|\chi_{\text{eff}}|}{\chi_0} = \frac{1}{2}(3 \cos^2 \theta - 1) \quad (5)$$

where  $\theta$  is the angle between the axis of rotation and the principal z-axis of the quadrupole coupling tensor, in this case the C-D axis.  $\chi_0$  is the zz-component of the static quadrupole interaction tensor. If the S-CD<sub>3</sub> unit describes a perfect tetrahedron,  $\chi_{\text{eff}} \sim 1/3\chi_0$ . A selection of line shapes calculated from these models is shown in Figure 3.

Between them, the five motional models cover all likely motions of a single DMSO molecule. If the precise values of jump angles and orientations of jump axes were to be different from the models, we would expect to arrive at similar, but not identical, spectra to those calculated. We were mindful of this when optimizing the fits.

## Results and Discussion

**XRD.** Variable-temperature XRD patterns of kaolinite:DMSO are shown in Figure 4. Intercalation results in a considerable portion of the clay expanding from a basal spacing  $d(001)$  of 7.17 to 11.26 Å. The proportion of clay expanded increases with the time of contact with DMSO.<sup>6</sup> The ratio

$$\frac{I_{(001)\text{complex}}}{I_{(001)\text{complex}} + I_{(001)\text{kaolinite}}}$$

is often used as a measure of the degree of intercalation, assuming approximately the same degree of particle orientation for both the expanded and unexpanded forms. The degree of intercalation of our samples approaches unity (see ref 9). This is supported by TGA measurements, which suggest for the intercalate a formula of  $\text{Al}_2\text{Si}_2\text{O}_5(\text{OH})_4(\text{DMSO})_n$  with  $n$  close to 1.

In the range 293–333 K no significant changes are observed in the powder patterns of the intercalate. The first changes occur between 333 and 353 K: (i) two reflections centered at about 4.1 Å coalesce into a single line; (ii) there are changes in the  $2\theta$  range 34–39°; (iii) lines in the  $2\theta$  range 44–50° virtually disappear.

(22) Mehring, M. In *NMR: Basic Principles and Progress*; Springer-Verlag: Berlin, 1976.

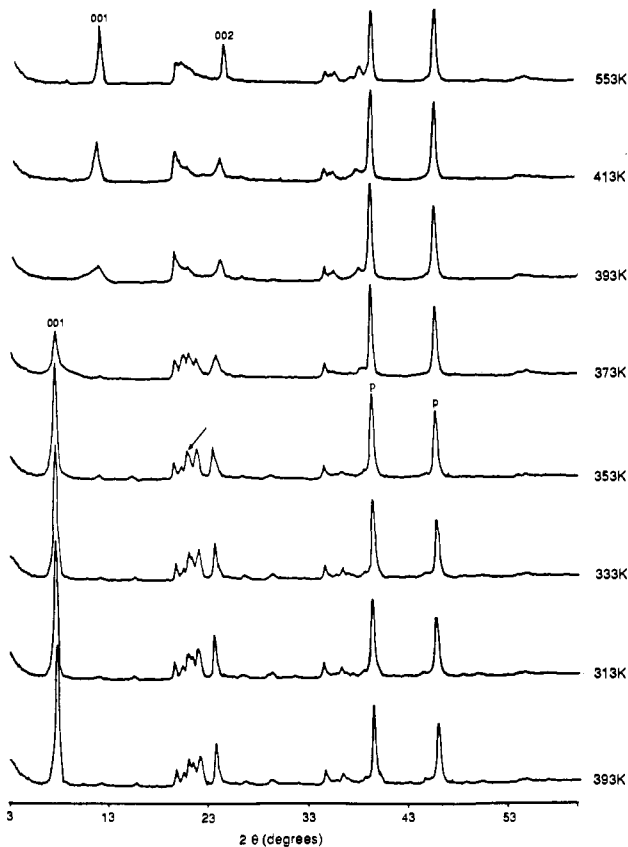


**Figure 4.** Results of a variable-temperature XRD study of the decomposition of the kaolinite:DMSO intercalate in a  $N_2$  atmosphere. The reflections labeled with p are of instrumental origin.

However, major changes in the patterns only occur above 353 K, the most obvious being the decrease in the height and broadening of the line at 11.26 Å. Between 373 and 393 K the intercalate collapses to a form of disordered kaolinite. Above 413 K only slight changes in the intensity of some lines, such as (001) and (002), are found. Quenching samples from 553 K to room temperature induces no changes in the XRD patterns. The powder pattern of the collapsed intercalate strongly resembles that of a poorly crystalline kaolinite, and it exhibits a characteristic "sharp rise, slow fall" in the  $2\theta$  range 19–26°, ascribed to layer stacking faults or layer-to-layer shifting of Al vacancies, and a lack of resolution of the peaks in the  $2\theta$  range 34–40°, due to defects originated by random translation of layers (see ref 23 and refs therein).

**$^2H$  NMR Spectra and Motion of the  $d_6$ -DMSO Molecule.**  $^2H$  NMR spectra recorded at temperatures between 160 and 415 K are shown in Figures 5–7. The immediate conclusion to be drawn is that all the methyl groups are in rapid motion about their respective C–S bonds: the line widths are too narrow for static  $CD_3$  groups ( $\chi_0 \sim 165$  kHz for  $^2H$  in a methyl group), but correspond well to those expected for rapidly rotating methyl groups ( $\chi_{eff} \sim 1/3\chi_0$ ).

None of the five motional models taken alone could reproduce the temperature and  $\tau$  dependence of the experimental spectra. In particular, none of the models with the exception of model 3 can reproduce the shoulders or wings at the outer edges of the powder pattern. Spectra calculated on the basis of the other four models do not show shoulders in the intermediate exchange regime, where the central part of the calculated powder pattern begins to resemble the experimental spectra. This cannot be corrected by varying jump angles or jump axes. On the other hand, although model 3 does generate shoulders at the outer edges at all hopping frequencies, the central part of the spectrum cannot be made to

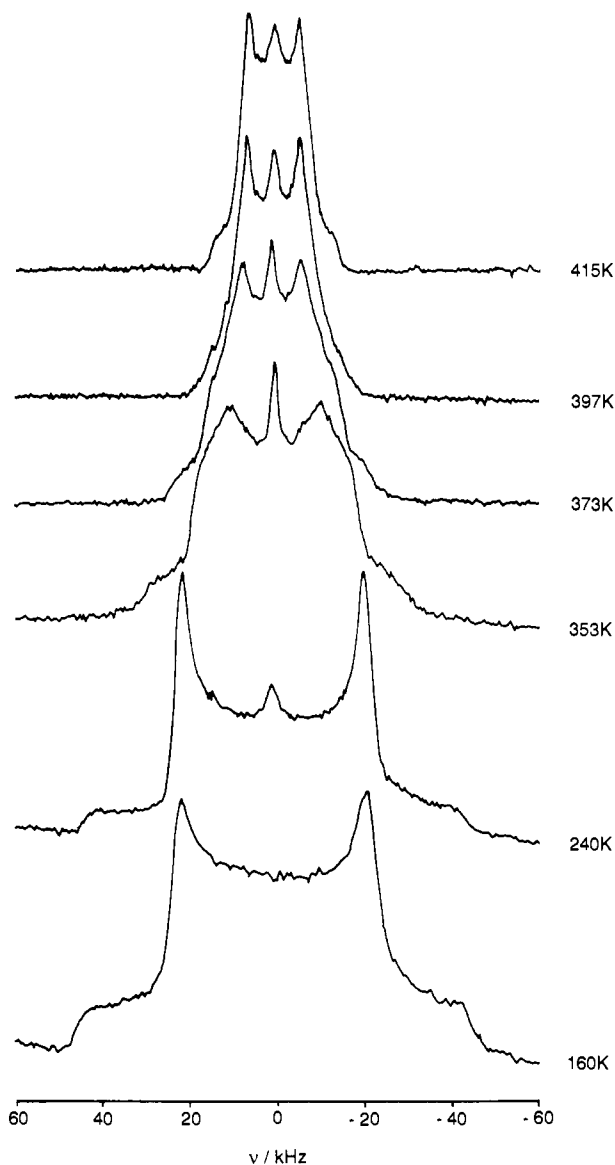


**Figure 5.** Selected  $^2H$  spectra of the kaolinite: $d_6$ -DMSO intercalate in the range 160–415 K, recorded with  $\tau_1 = 25$   $\mu s$ . Further spectra in the range 303–343 K are given in Figures 6 and 7. Note that between 240 and 303 K the spectra do not change significantly.

resemble the experimental spectrum for any choice of axes and frequencies. The fact that when the temperature is increased from 298 to 339 K the two  $^{13}C$  resonances begin to coalesce (see below) is consistent with exchange between two different methyl sites. We therefore attempted to fit the experimental  $^2H$  spectra assuming the presence of two different types of methyl groups with independent motions of different types. The variation of the line shape with  $\tau$  is of central importance to the fitting of the spectra. Satisfactory fits were found for one  $^2H$  site moving according to model b with an added "static"  $^2H$  site in the population ratio 1:1 for the temperature range 160–333 K. By "static" we mean that there is no motion other than the rapid spinning of the methyl groups about the S–Me bond, which is assumed in all models. The calculated spectra which best fit the experimental spectra in the range 303–333 K are shown in Figure 6 (fit 1). Model b (jump angle 109.5°) involves frequencies in the range 150–1200 kHz for this temperature range. The effective quadrupole coupling constant associated with model b is 59 kHz, compared with 67 kHz for the static  $^2H$  site. While the difference in quadrupole coupling constants may in part reflect different chemical environments between the two sites, it is more likely to reflect different geometries of the methyl groups. The quadrupole coupling constant is relatively insensitive to small changes in chemical environment. However, rapid rotation of the methyl group reduces

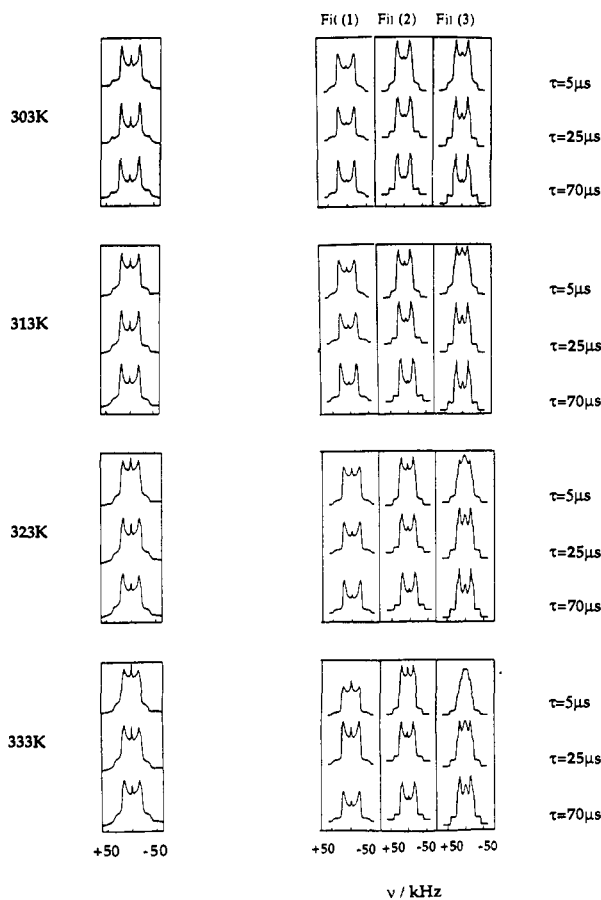


Figure 6. Comparison between experimental and simulated  $^2\text{H}$  line shapes in the range 303–333 K. Spectra were recorded with  $\tau_1 = 5, 25,$  and  $70 \mu\text{s}$ . The details of the three acceptable fits shown are given in Table I.

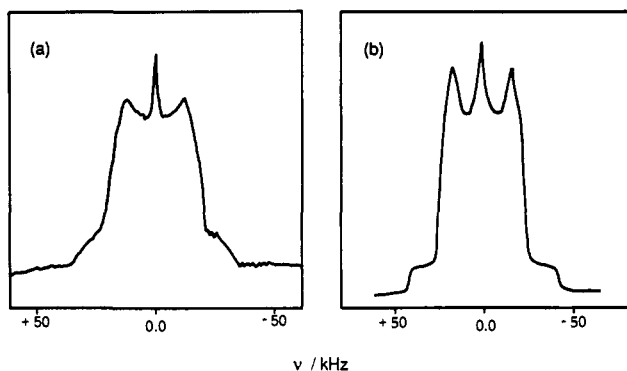


Figure 7. Comparison between the best-fit  $^2\text{H}$  simulation with the experimental line shape at 343 K ( $\tau = 5 \mu\text{s}$ ). As a result of exchange between the two  $^2\text{H}$  sites, the fits gradually deteriorate above 333 K.

the quadrupole coupling constant  $\chi_0$  (see eq 5). Variation in  $\theta$ , the angle between the hopping C–D bond and the rotation axis, by only  $3\text{--}4^\circ$  between the two sites can cause this difference in effective quadrupole coupling. In turn, variation in  $\theta$  of  $3\text{--}4^\circ$  between two sites seems eminently possible for an intercalated species. If we assume the quadrupole coupling constant for  $^2\text{H}$  in  $d_6$ -DMSO to be 165 kHz, then an S–C–D angle of  $104.5^\circ$  for the static site and  $108^\circ$  for the moving site would give effective quadrupole coupling constants of 67 and 59 kHz, respectively. For example, if the methyl groups of one site were partially keyed into the kaolinite layer as has been proposed,<sup>11,12</sup> and the other DMSO site contained a motionally free molecule in the interlayer spacing, we would expect some significant differences in the geometries of the methyl groups for the two sites.

It is difficult to calculate exactly the hopping frequency associated with model b below 300 K with any degree of precision,

Table I. Fits of Simulated and Experimental Line Shapes<sup>a</sup>

temp/K	fit 1		fit 2		fit 3	
	site 1 <sup>b</sup>	site 2	site 1 <sup>c</sup>	site 2	site 1 <sup>d</sup>	site 2
303	150		150		150	
313	300		300		300	
323	600	static	600	10 000	600	10 000
333	1200		1200		1200	

<sup>a</sup> The frequencies of the molecular hops are given in kilohertz. <sup>b</sup> Site 1: jump angle  $109^\circ$ , two sites (model b); tolerance,  $\pm 100$  kHz. Site 2: static. <sup>c</sup> Site 1: jump angle  $109^\circ$ , two sites (model b); tolerance,  $\pm 100$  kHz. Site 2: jump angle  $141^\circ$ , two sites (model c); tolerance, motion in high-speed limit. <sup>d</sup> Site 1: jump angle  $109^\circ$ , three sites (model a); tolerance,  $\pm 100$  kHz. Site 2: jump angle  $141^\circ$ , two sites (model c); tolerance, motion in high-speed limit.

because there is very little variation in line shape with  $\tau$  or frequency for hopping frequencies below 100 kHz, this being the approach of the slow-motion limit. The experimental spectra reflect this, changing very little with temperature or with  $\tau$ .

A comparison of the calculated and experimental spectra in Figure 6 reveals that the zero-frequency feature of the experimental spectra is not faithfully reproduced by the calculations. Below 323 K, this feature is always calculated to be lower in intensity than is observed experimentally. This is probably due to the presence of very small quantities of free DMSO in the samples. Indeed, the intensity of this central feature was found to vary slightly between individual samples.

Acceptable fits were also obtained from one  $^2\text{H}$  site moving according to model b + one site moving according to model c in the ratio 1:1 (Figure 6, fit 2). Here, the quadrupole coupling constant is 59 kHz for model b and 67 kHz for model c. Model a + model c in the ratio 1:1 also produces an acceptable fit (Figure 6, fit 3), but less good at the higher temperatures. The quadrupole coupling constants are 59 kHz for model a and 67 kHz for model c. The hopping frequencies that gave rise to the calculated spectra in Figure 6 are given in Table I.

At 343 K and above, the experimental spectra could not be fitted satisfactorily. It is interesting to note that the first changes in the XRD patterns and IR spectra occur at similar temperatures. Figure 7 shows the best fit obtained for the 343 K  $^2\text{H}$  NMR spectrum ( $\tau = 5 \mu\text{s}$ ), this being with model b + model c. Although the calculated spectrum has all the features of the experimental spectrum, the latter is much broader. Simple line broadening of the calculated spectrum does not, however, reproduce the experimental spectrum. Clearly, at 343 K and above there is some further exchange process causing broadening; this may well involve the "unlocking" of a methyl group of the DMSO. This molecular exchange process may trigger the early changes in the long-range order of the intercalate.

Above 415 K, the  $^2\text{H}$  spectra show no further changes (cf. similar result obtained from the XRD study). Inspection of the  $^2\text{H}$  spectrum at 415 K (Figure 5) shows it to contain two components: a broad feature at zero frequency, and a static-like powder pattern, but considerably narrowed in comparison with the lower temperature spectra. The effective quadrupole coupling constant for the  $^2\text{H}$  spins determines the width of the powder pattern. In turn, eq 5 quantifies the decrease in the effective quadrupole coupling constant resulting from rapid rotation of the  $^2\text{H}$  nuclei about an axis inclined at an angle  $\theta$  to the principal z-axis of the quadrupole coupling tensor. The line narrowing that occurs between the lower temperature (160–333 K) and the higher temperature (above 373 K)  $^2\text{H}$  spectra corresponds to the methyl groups rotating about an axis inclined at ca.  $70^\circ$  to the Me–S bonds, in addition to their rapid spinning about the Me–S bonds, which occurs throughout the whole temperature range studied. This motion would seem to correspond to the DMSO molecules spinning rapidly about their approximate pyramid axis. This implies that above 415 K all those DMSO molecules that remain in the interlayer spacing are essentially free and not keyed into the kaolinite layer. The broad feature at zero frequency is probably due to free DMSO molecules outside the interlayer spacing.

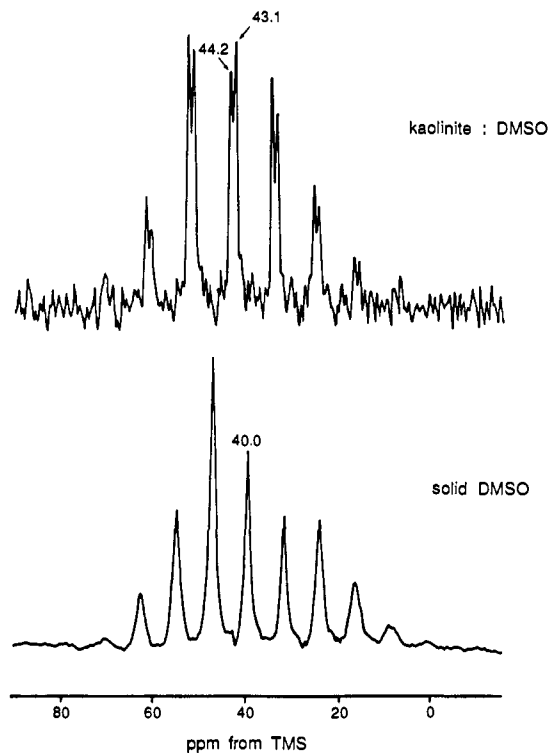


**Figure 8.**  $^{13}\text{C}$  HPDC NMR spectra of solid DMSO (213 K) and the intercalate recorded with spinning rates of ca. 800 and 900 Hz, respectively. The arrows depict the isotropic chemical shift.

Our analysis of the  $^2\text{H}$  NMR spectra assumes that there is no preferred orientation of kaolinite particles. Although we have taken steps to avoid preferred orientation (by using fine grinding, varying degrees of compactness of the sample, and different geometries of sample containers and checking the reproducibility of the results), this possibility must nonetheless be considered. Evidence for the absence of preferred orientation comes from the spectrum measured at 160 K (Figure 5), which is a typical, symmetric static  $^2\text{H}$  powder pattern. The spectrum taken at 415 K is again a classic deuterium spectrum with a central line from mobile DMSO. This can only happen when the distribution of particles is isotropic.

**Other NMR Results.** The  $^1\text{H}$ - $^{13}\text{C}$  CP/MAS and HPDC spectra of kaolinite:DMSO (Figures 8 and 9) contain two resonances at 43.1 and 44.2 ppm. These have been assigned by other workers<sup>11,12</sup> to two inequivalent  $^{13}\text{C}$  atoms in the same DMSO molecule: one methyl group is thought to be keyed into the ditrigonal holes in the silicate sheet, the other being approximately parallel to the sheet. Thompson and Cuff<sup>11</sup> suggested that the two methyl carbons could be inequivalent due to a small difference in the C-S bond lengths as found in solid DMSO (0.05 Å).<sup>24</sup> However, a static  $^{13}\text{C}$  study of solid DMSO<sup>25</sup> detected only a single resonance at 40 ppm. Thus, the doublet observed in the spectrum of kaolinite:DMSO probably does not arise from a small difference in the C-S bond lengths such as that reported for solid DMSO. Alternatively, we may assign the two  $^{13}\text{C}$  resonances to two different DMSO sites within the unit cell.

Spin-lattice relaxation measurements using the pulse sequence proposed by Torchia<sup>26</sup> show that the 44.2 ppm resonance has a significantly longer relaxation time ( $264 \pm 30$  ms and  $390 \pm 40$  ms for the 43.1 and 44.2 ppm resonances, respectively), in agreement with ref 12. Variable-temperature  $^{13}\text{C}$  CP/MAS studies (Figure 9) show that when the temperature is increased from 298 to 339 K, the two  $^{13}\text{C}$  resonances of the intercalate shift

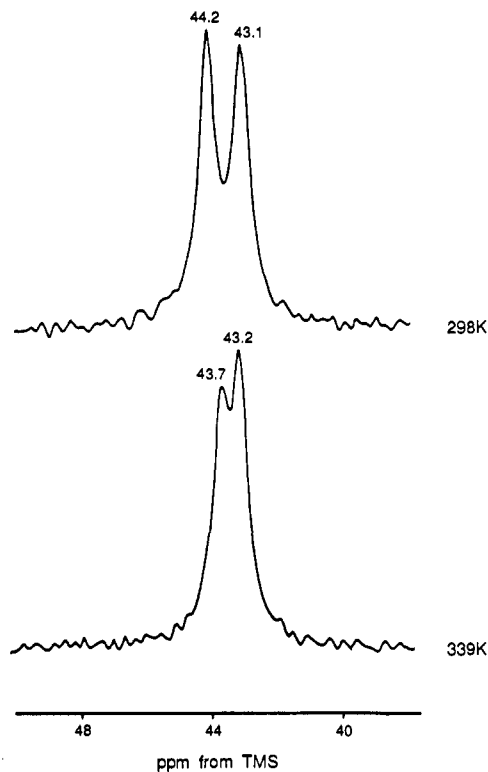


**Figure 9.** Temperature dependence of the  $^1\text{H}$ - $^{13}\text{C}$  CP/MAS NMR spectrum of the intercalate.

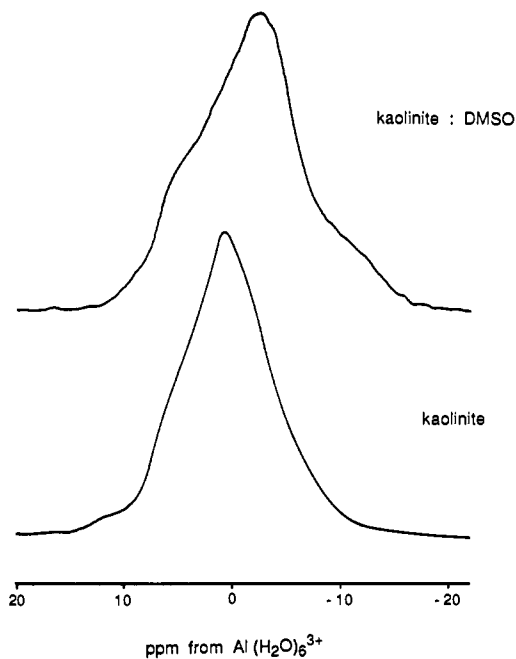


**Figure 10.**  $^{27}\text{Al}$  HPDC NMR spectra of kaolinite and the intercalate.

from 44.2 and 43.1 ppm to 43.7 and 43.2 ppm, respectively, and the intensity of the lower frequency resonance increases slightly. The 3–4 ppm shift to high frequency of the DMSO resonance relative to pure solid DMSO supports an interaction between the sulfur atom of DMSO and the oxygens of the  $\text{SiO}$  matrix of kaolinite. The slow convergence of the two  $^{13}\text{C}$  resonances could be due to the onset of exchange between two  $^{13}\text{C}$  sites. Note that rapid random motion ensures that non-intercalated DMSO molecules do not give rise to a third resonance in the  $^1\text{H}$ - $^{13}\text{C}$  CP/MAS spectrum of the intercalate. On the other hand, a third  $^{13}\text{C}$  resonance at ca. 40.1 ppm in the spectra recorded with HPDC has been observed.<sup>10</sup> Due to the very careful outgassing procedure used, this signal was not seen in the HPDC spectra of our samples.

(24) Thomas, R.; Schoemaker, C. B.; Eriks, K. *Acta Crystallogr.* **1966**, *21*, 72.

(25) Pines, A.; Gibby, M. G.; Waugh, J. S. *Chem. Phys. Lett.* **1972**, *15*, 373.

(26) Torchia, D. A. *J. Magn. Reson.* **1978**, *30*, 613.

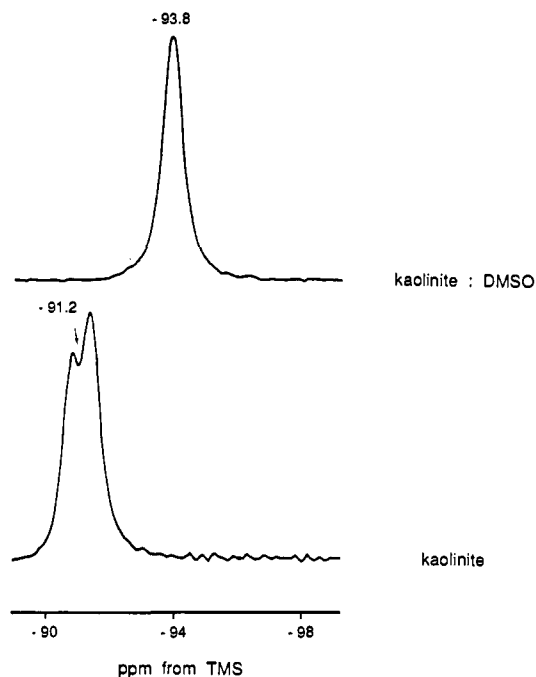


Figure 11.  $^1\text{H}$ - $^{29}\text{Si}$  CP/MAS NMR spectra of kaolinite and the intercalate.

However, the relatively poor signal-to-noise ratio of these spectra precludes the detection and quantification of a small amount of free DMSO.

The  $^{27}\text{Al}$  MAS NMR spectra of kaolinite and its DMSO intercalate recorded with  $^1\text{H}$  HPDC are shown in Figure 10. In both spectra, and particularly in the latter, a second-order quadrupole line shape is evident. Due to line broadening caused by strong  $^1\text{H}$ - $^{27}\text{Al}$  dipolar coupling, these line shapes are not at all distinct when no  $^1\text{H}$  decoupling is used, and this explains why others failed to detect the difference between the  $^{27}\text{Al}$  spectrum of kaolinite and that given by the intercalate.<sup>11</sup> The spectra clearly show that the  $\text{AlO}_6$  octahedra in the intercalate are more distorted ( $C_Q = 4.1 \pm 0.1$  MHz,  $\eta = 0.8 \pm 0.2$ ) than in kaolinite ( $C_Q = 3.5 \pm 0.1$  MHz,  $\eta = 0.8 \pm 0.2$ ).<sup>27</sup>

The  $^{29}\text{Si}$ - $^1\text{H}$  CP/MAS spectrum of kaolinite (Figure 11) is a doublet centered at  $-91.2$  ppm with a full width at half-maximum of 94 Hz. The kaolinite:DMSO intercalate gives a single, narrower (58 Hz), resonance at  $-93.8$  ppm, suggesting a higher degree of order in the intercalate than in the siliceous matrix of kaolinite. The increased shielding of the intercalate resonance relative to the kaolinite doublet indicates the presence of an electron-withdrawing interaction between the sulfur atom of DMSO and the oxygens of the siliceous matrix of kaolinite, which might arise from the  $\text{S}^+-\text{O}^-$  nature of the  $\text{S}=\text{O}$  bond in the DMSO. The degeneracy of the silicon environments caused by the expansion of the kaolinite structure suggests that interlayer hydrogen-bonding effects are the principal cause of Si site differentiation in kaolinite.<sup>10</sup>  $^{29}\text{Si}$  NMR spectroscopy also confirms that the degree of intercalation of the samples approaches unity.

**Infrared Spectroscopy.** In general, our FTIR results (Figure 12) are in accordance with previous reports,<sup>6,8,12</sup> but we report one new band previously not observed and also the results of deuterating the kaolinite:DMSO lattice. The results lead to three related conclusions, which are summarized below. We do not discuss the details of assignment and interpretation here, as this has been dealt with extensively in ref 12.

(i) **The DMSO molecule is hydrogen-bonded to the clay hydroxyls.** Intercalation of DMSO into kaolinite leads to an appreciable decrease of the intensity of the hydroxyl band of kaolinite at  $3695\text{ cm}^{-1}$  and to the appearance of sharp peaks at  $3663$ ,  $3546$ , and  $3505\text{ cm}^{-1}$  (also seen in the same region of the spectrum of

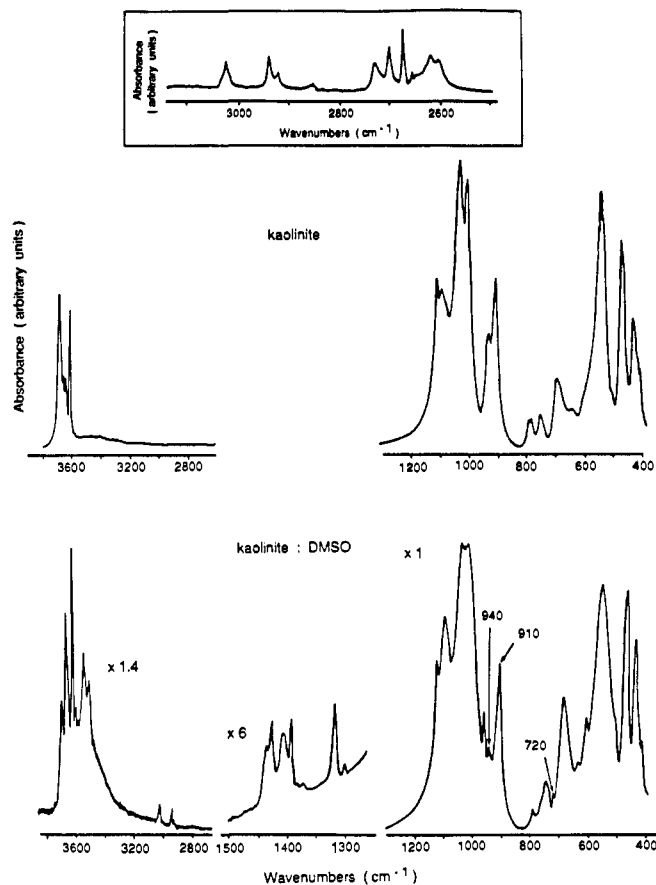


Figure 12. FTIR spectra of kaolinite and the intercalate. The inset shows a selected region of the *d*-kaolinite:DMSO spectrum.

*d*-kaolinite:DMSO), attributed to the formation of moderately strong hydrogen bonds between some of the inner-surface hydroxyls, facing the interlayer space of kaolinite and the sulfonyl oxygen.<sup>8</sup> In addition to the five bands usually reported in the hydroxyl region of the spectrum of kaolinite:DMSO, our spectrum shows a new, very sharp band at  $3599\text{ cm}^{-1}$ . Deuteration of kaolinite:DMSO produces six new bands in the range  $2730$ – $2600\text{ cm}^{-1}$ . The  $\nu_{\text{OH}}:\nu_{\text{OD}}$  frequency ratio is about 1.35. Moreover, upon intercalation with DMSO the intensity of the Al-OH vibrations at  $940$  and  $910\text{ cm}^{-1}$ , particularly the former, decreases.

(ii) **The DMSO hydrogen bonds via the oxygen rather than the sulfur atom.** Olejnik et al.<sup>6</sup> examined a thin sample of kaolinite:DMSO and concluded that the two bands in the range  $1040$ – $1018\text{ cm}^{-1}$  are probably composed of three overlapping peaks. One of these, centered at around  $1030\text{ cm}^{-1}$ , was assigned to the S-O stretch in the complex ( $1057\text{ cm}^{-1}$  in liquid DMSO). The downward frequency shift of the S-O stretching vibration suggests that the DMSO tends toward the  $(\text{CH}_3)_2\text{S}^+-\text{O}^-$  resonance form, which supports the bonding via the oxygen atom. On the other hand, a peak at  $720\text{ cm}^{-1}$  in the kaolinite:DMSO complex was assigned to the asymmetric C-S stretching which in liquid DMSO occurs at  $699\text{ cm}^{-1}$ . The absence of the symmetric C-S vibration may be explained by a lowering of the DMSO symmetry after intercalation<sup>10</sup> and suggests that the two methyl carbons may be inequivalent.

(iii) **The DMSO methyl groups do not interact with the kaolinite SiO matrix.** The lines at  $1445$  and  $1414\text{ cm}^{-1}$  corresponding to asymmetric CH bending modes in liquid DMSO are replaced by three lines at  $1428$ ,  $1408$ , and  $1394\text{ cm}^{-1}$  in the intercalate. In addition, the symmetric CH stretching vibration shifts from  $2994$  and  $2913\text{ cm}^{-1}$  (liquid DMSO) to  $3022$  and  $2936\text{ cm}^{-1}$  and a shoulder appears at  $2919\text{ cm}^{-1}$ . It is clear that the high-frequency shift of the CH stretching vibration does not support CH...O bonding to the tetrahedral oxygen layer, but may reflect an increase in C-H bond strength brought about by the increased positive charge on S. The IR spectra of kaolinite:DMSO begin

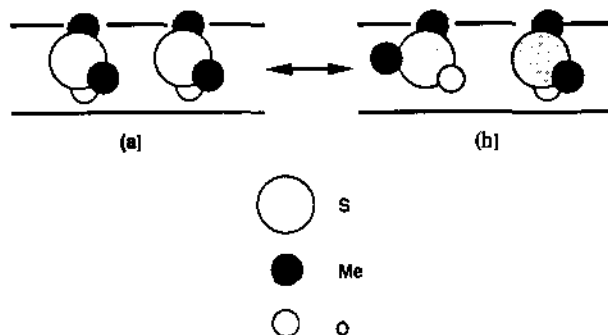


Figure 13. A schematic diagram showing the proposed motion of the DMSO molecule arising from analysis of the static  $^2\text{H}$  spectra (fit 1).

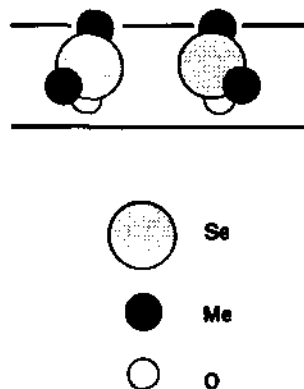


Figure 14. A schematic diagram illustrating the orientation of DMSO molecules<sup>11</sup> in the kaolinite:DMSO intercalation compound with the interlayer spacing of 11.38 Å.

to show significant changes above 338 K.<sup>6</sup>

#### Conclusions

$^2\text{H}$  NMR spectroscopy shows that there are two different  $^2\text{H}$  sites for the  $d_6$ -DMSO molecule in the interlayer space. There are three possible fits of simulated and experimental  $^2\text{H}$  spectra. Two of these (fits 2 and 3) require both  $^2\text{H}$  sites to be involved

in different motions, in such a way that they cannot belong to the same DMSO molecule. Fit 1 involves a static and a mobile  $^2\text{H}$  site; only in this case could the two sites belong to the same molecule. As is illustrated schematically in Figure 13, if one methyl group of the DMSO molecule were keyed into the kaolinite host, it might appear static, while the "free" methyl group could hop between different positions. In this particular fit, the "free" methyl group hops between just two sites, which are angled  $109^\circ$  apart. It is reasonable to ask why the DMSO molecule does not spin all the way around the "keyed" methyl-S bond. We can begin to answer this question by reference to the three intercalation compounds formed by DMSO with kaolinite.<sup>12</sup> One of these intercalation compounds has an interlayer spacing of 11.26 Å, and the DMSO molecules are oriented in a similar fashion to the DMSO molecules in Figure 13a. The kaolinite:DMSO compound appears to be analogous to this compound.<sup>12</sup> A second intercalation compound has an interlayer spacing of 11.38 Å.<sup>12</sup> The orientation of the DMSO molecules in this compound is shown in Figure 14. It would thus appear that rotating one DMSO molecule so that the Se lone pair faces the Se lone pair on the neighboring molecule requires an expansion of the interlayer spacing. If this result can be transferred to the kaolinite:DMSO compound, it is easy to see why the DMSO molecule does not spin freely about the "keyed" Me-S bond: such motion would be subject to a very large activation energy, if it involved the expansion and contraction of the interlayer spacing. The experimental  $^2\text{H}$  spectra also show that all the methyl groups are in rapid motion about their respective C-S bonds.

Above 343 K, XRD patterns and  $^2\text{H}$  NMR spectra show significant changes. In addition, the two resonances observed in the  $^{13}\text{C}$  spectrum begins to coalesce at around the same temperature. The changes in the  $^2\text{H}$  spectra are interpreted as arising from exchange between the two methyl groups: this must involve a periodic "unkeying" of one methyl group from the kaolinite layer. We are investigating the possibility that this exchange promotes the structural changes in the kaolinite lattice observed in the XRD experiment. Above 415 K, all DMSO molecules remaining in the interlayer space appear to be in one site and are rapidly rotating approximately about the pyramid axis of the molecule.

**Acknowledgment.** We are grateful to Unilever Research, Port Sunlight, the University of Aveiro, and the Royal Society for support and to Dr. A. Lurf for comments on the manuscript.